Available online at www.sciencedirect.com
SCIENCE DIRECT
Journal of Magnetic Resonance 180 (2006) 18–28
JMR Journal of Magnetic Resonance
www.elsevier.com/locate/jmr

Fast imaging with the MMME sequence

H. Cho, L. Chavez [1], E.E. Sigmund, D.P. Madio, Y.-Q. Song *

Schlumberger-Doll Research, 36 Old Quarry Road, Ridgefield, CT 06877, USA

Received 25 October 2005; revised 22 December 2005
Available online 20 January 2006

Abstract

The multiple-modulation-multiple-echo sequence, previously used for rapid measurement of diffusion, is extended to a method for single shot imaging. Removing the gradient switching requirement during the application of RF pulses by a constant frequency encoding gradient can shorten experiment time for ultrafast imaging. However, having the gradient on during the pulses gives rise to echo shape variations from off-resonance effects, which make the image reconstruction difficult. In this paper, we propose a simple method to deconvolve the echo shape variation from the true one-dimensional image. This method is extended to two-dimensional imaging by adding phase encoding gradients between echoes during the acquisition period to phase encode each echo separately. Slice selection is achieved by a frequency selective pulse at the beginning of the sequence. Imaging speed is mainly limited by the phase encoding gradients' switching times and echo overlap when echo spacing is very short. This technique can produce a single-shot image of sub-millimeter resolution in 5 ms.

Keywords: MMME; Fast imaging; Multiple echoes; Off-resonance effects

1. Introduction

There exist a wide-range of interests and methods for ultrafast NMR image acquisition. Echo planar imaging (EPI) [1] and fast low angle shot (FLASH) [2] type sequences drastically reduce image acquisition time but require rapidly switched high gradient pulses as these methods rely on gradient echoes. Due to the heavy dependence on the gradient system, it is well known that these methods are susceptible to magnetic field inhomogeneities (mainly for EPI) and eddy currents artifacts from rapidly switched high field gradients. The RARE (rapid acquisition with relaxation enhancement, also known as TSE or FSE) [3] sequence uses many π RF pulses and gradient switchings to periodically refocus the spin magnetization, which may lead to excessive RF energy deposition.

There has been growing interest in PREVIEW [4], QUEST [5,6], and DUFIS type [7–11] sequences for acquiring draft-quality images because these sequences generally require less gradient switching and use multiple spin echoes generated from relatively few RF pulses for fast image acquisition. However, the limited number of echoes in the above sequences generally make it difficult to obtain high resolution images.

The generation of multiple echoes by a combination of magnetic field gradient and a few RF pulses is well described by a coherence pathway formalism. Consider a four pulse sequence (multiple-modulation-multiple-echo (MMME4)) with [90° −90° −90° −180°] flip angles in the presence of a constant field gradient as shown in Fig. 1 [12,13]. A magnetic field gradient can create a periodic modulation of the spin magnetization, while the RF pulses cause a rotation that mixes transverse and longitudinal components of spin magnetization. As a result, there exist a large number of coherence pathways when even a small number of RF pulses are applied in the presence of a field gradient. It is well known that the

* Corresponding author. Fax: +1 203 438 3819.
E-mail address: ysong@slb.com (Y.-Q. Song).
[1] Present address: Department of Chemistry, University of California, Berkeley, CA 94720, USA.

1090-7807/$ - see front matter © 2006 Elsevier Inc. All rights reserved.
doi:10.1016/j.jmr.2005.12.014

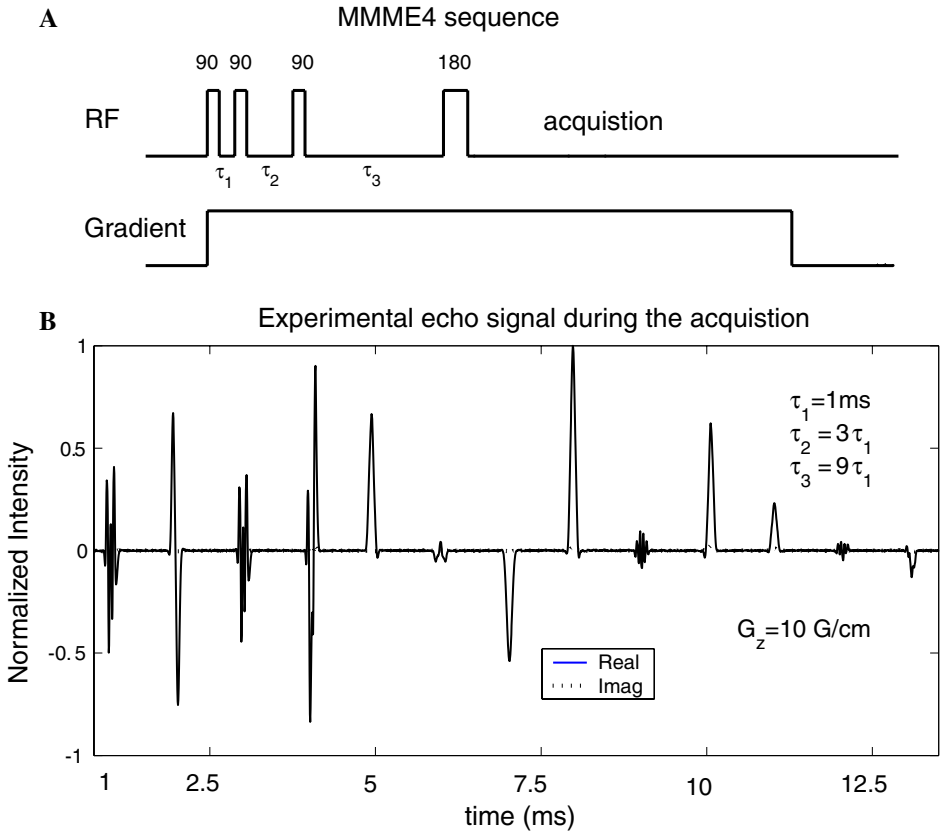

Fig. 1. A four pulse sequence (MMME4) in the presence of a constant field gradient (A). Experimental echo signals after the last pulse (π pulse) with [90° −90° −90° −180°] flip angles with the z gradient are shown (B). Echo signals from the imaginary part are made negligibly small by setting the phase of all pulses to zero [13].

different coherence pathways with N RF pulses can generate as many as,

$$n = \frac{3^{(N-1)} - 1}{2} + 1, \quad (1)$$

observable signals [12–15]. These multiple echoes can be easily set to appear at well separated times during the acquisition period because the echoes appear only when the total acquired phase is zero. For example, Fig. 1 shows 13 well-separated echoes from the MMME4 sequence.

This advantage has been utilized in recent work for one-shot measurement of diffusion based on the MMME sequence [13,16,17]. Previous ultra-fast imaging methods such as PREVIEW, QUEST, and DUFIS-type sequences also rely on the generation of multiple echoes from a small number of RF pulses as mentioned earlier.

Ideally, for both higher speed and signal-to-noise ratio (SNR) for ultrafast imaging applications, it is desirable to have no gradient switching and high flip angle pulses. DUFIS uses a string of low-flip angle pulses in the presence of a constant magnetic field gradient to achieve ~20 ms scan time [7]. The major limitation of this technique is relatively poor signal-to-noise ratio from using small flip angle pulses. QUEST-type experiments use high flip angle pulses, but turn the gradients off during the pulses and have longer scan times on the order of hundreds of milliseconds [5,6].

The MMME imaging sequence combines the advantages of these two techniques by employing high flip angle pulses without gradient switching along the frequency encoding direction. However, having the gradient on during the high flip angle pulses gives rise to echo shape variations among different echoes from off-resonance effects, which makes the image reconstruction challenging. In this paper, we propose a simple method to deconvolve these echo shape variations from the true one-dimensional (1-D) image for every echo arising from the MMME sequence.

We show that this method can be extended to two-dimensional (2-D) imaging by separate phase encoding of each echo signal. Slice selection is achieved using an extra-slice magnetization destruction scheme at the beginning of the pulse sequence.

2. Theory and pulse sequence

2.1. Echo shapes

In the presence of a static magnetic field gradient, the spin precession frequency linearly depends on position. This dependence leads to a spatial sinusoidal modulation

of spin magnetization in the sample, and this modulation is often described by k (spatial wave number),

$$k_u = \gamma \int \frac{\partial B_z}{\partial u}\,\mathrm{d}t, \tag{2}$$

where u is the direction of the applied field gradient.

For conventional 1-D NMR imaging, the time domain NMR signal in the presence of a field gradient (along the x direction) is related to the real-space image ($\rho(x)$, a spin density along the x direction) by a Fourier relationship, which can be expressed as

$$S = \int \rho(x)\mathrm{e}^{-\mathrm{i}k_x x}\,\mathrm{d}x. \tag{3}$$

For the MMME sequence with a constant field gradient and pulses of constant amplitude, each echo originates from a different coherence pathway. Eq. (3), without considering relaxation and decay due to diffusion, is modified to

$$S_{\mathrm{echo}} = \int \rho(x) f^{\mathrm{echo}}(\Delta\omega_0, \omega_1, t_p, \phi, N)\mathrm{e}^{-\mathrm{i}k_x x}\,\mathrm{d}x, \tag{4}$$

where S_{echo} is the acquired signal of each echo and $f^{\mathrm{echo}}(\Delta\omega_0, \omega_1, t_p, \phi, N)$ is generally a complex function for each echo. $\Delta\omega_0(x)$ represents the Larmor frequency offset from the RF frequency (ω_{RF}), $\Delta\omega_0(x) = \gamma|B_0 + \frac{\partial B_z}{\partial x}\mathrm{d}x| - \omega_{\mathrm{RF}}$ and $\omega_1 = \gamma B_1$. t_p, ϕ, and N are the duration, phase and number of pulses in the MMME sequence, respectively [13,18,19].

Without the field gradient during the RF pulse, $\Delta\omega_0 = \gamma|B_0| - \omega_{\mathrm{RF}}$ becomes a constant value. In this case, f^{echo} no longer varies across the sample, and only amplitude and phase variation exist among different echoes. These variations can be corrected either theoretically or empirically [13,16,4–6].

With the field gradient on during the RF pulse, f^{echo} is spatially dependent because $\Delta\omega_0$ becomes a function of position x (i.e., an RF pulse becomes slice-selective along the gradient direction). This off-resonance contribution gives rise to echo shape variation among different echoes and cannot be neglected for image reconstruction as we can see from the experimental echo signals shown in Fig. 1 [13]. Amplitude and phase correction schemes [4–6] may not be adequate in this case because there still remain uncompensated variations in echo shape among different echoes. In the MMME imaging method proposed here, the field gradient is on during the RF pulse and f^{echo} is spatially dependent.

To reconstruct the true 1-D image profile of interest from different echoes of the MMME sequence, we rewrite Eq. (4) as

$$S_{\mathrm{echo}} = \mathscr{F}(\rho(x)) \otimes \mathscr{F}(f^{\mathrm{echo}}), \tag{5}$$

where $\mathscr{F}$ represents Fourier transform and $\otimes$ is convolution.

To obtain the true image ($\rho(x)$), it is necessary to deconvolve the echo shape contribution ($\mathscr{F}(f^{\mathrm{echo}})$) from the signal of the individual echo (S_{echo}). We utilize a simple Fourier relationship to achieve this deconvolution.

From Eq. (5), a 1-D image can be reconstructed through

$$\rho(x) = \frac{\mathscr{F}^{-1}(S_{\mathrm{echo}})}{f^{\mathrm{echo}}}. \tag{6}$$

f^{echo} can be either calculated theoretically [13] or empirically by performing a reference scan with an infinitely long sample. For an infinitely long sample, Eq. (5) reduces to

$$S^{\mathrm{ref}}_{\mathrm{echo}} = \delta(x) \otimes \mathscr{F}(f^{\mathrm{echo}}) = \mathscr{F}(f^{\mathrm{echo}}). \tag{7}$$

By substituting Eq. (7) into Eq. (6) one gets

$$\rho(x) = \frac{\mathscr{F}^{-1}(S_{\mathrm{echo}})}{\mathscr{F}^{-1}(S^{\mathrm{ref}}_{\mathrm{echo}})}. \tag{8}$$

This method also can compensate for echo signal decay due to uniform relaxation and diffusion, which was not explicitly accounted for in Eq. (4). However, if both relaxation and diffusion are heterogeneous, the correction will become more difficult.

For 2-D imaging, a train of small blipped gradients can be switched between successive echoes to phase encode each echo separately in the presence of a constant frequency encoding gradient.

2.2. Pulse sequence

In general, the N RF pulse sequence (MMMEN) can provide exponentially increasing number of echoes for 2-D imaging as N gets large. However, T_2 relaxation and decay due to diffusion tend to decrease the SNR of later echoes in the time domain as we introduce more RF pulses.

Here, we describe a 2-D imaging method for the MMME5 sequence as shown in Fig. 2. An extension of this method is applicable to any MMMEN sequences if necessary. Five hard pulses are applied in the presence of a constant frequency encoding gradient (G_x) to create 40 echoes after the last pulse. Additional echo signals (1, 4, and 13 echoes during τ_2, τ_3, and τ_4 periods, respectively) can also be used for image reconstruction. Acquisition of these echoes during the delay between the RF pulses may be important in a situation where the SNR of later echoes are relatively low.

For the phase encoding gradients (G_y), small blipped gradients are applied between successive echoes. Higher amplitude echoes can be used to encode the central portion of k-space. The strength of each blip gradient (ΔG_y) is $\leqslant$1 G/cm, and five higher gradient lobes are used to arrange the optimal order of k-space encoding. For instance, Fig. 3 shows the k-space trajectories in the MMME4 and MMME5 sequences for 2-D imaging.

Slice selection (G_z) is achieved using an extra-slice magnetization destruction scheme at the beginning of the pulse sequence. This method is advantageous for our imaging sequence because it can minimize the gradient switching requirement during the RF pulses. We tested both a DIGGER pulse (sine–sinc function) [20–22] and a soft pulse generated by MATPULSE [23] based on the Shinnar-Le Roux algorithm [24].

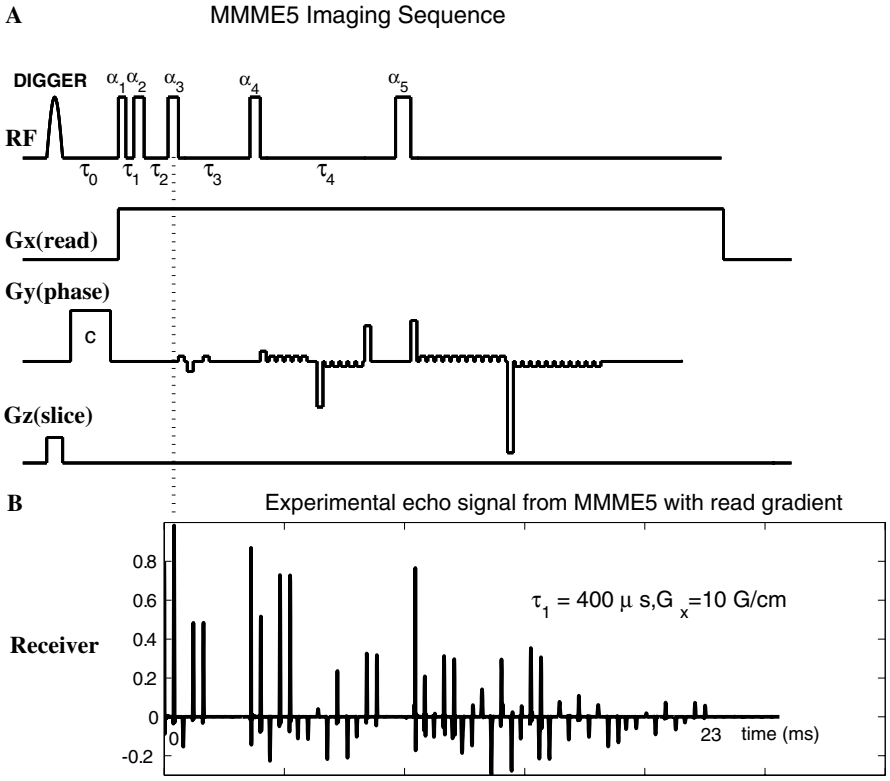

Fig. 2. A five pulse sequence (MMME5), used for 2-D imaging with slice selection (A). Experimental echo signals with [54° −71° −71° −71° −110°] flip angles with the x (read) gradient are shown (B).

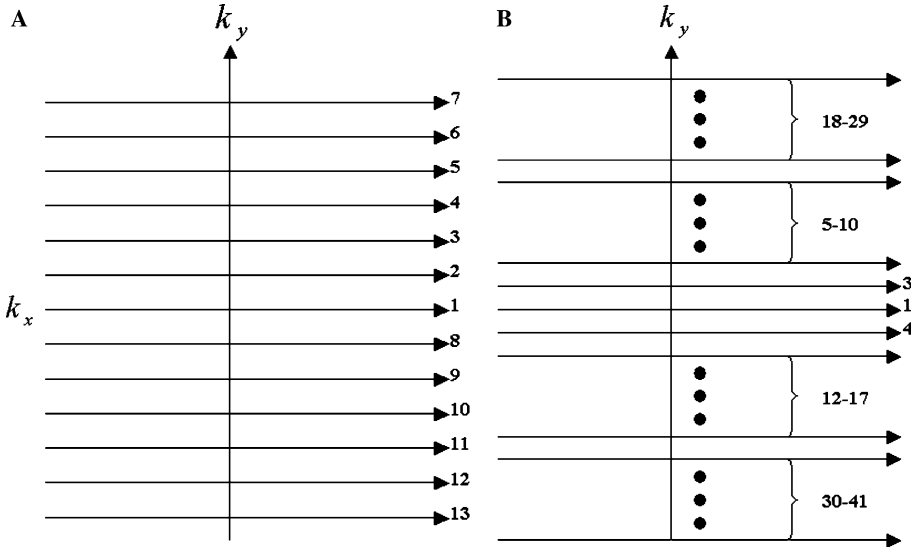

Fig. 3. Optimized k-space trajectories of the MMME imaging sequence. Numbers represent the echo number from the MMME4 (A) and MMME5 (B) in sequential order in the time domain acquisition. Higher amplitude echoes are used to encode the central portion of k-space.

3. Experimental results and discussion

3.1. Experimental setup

A schematic diagram of the experimental setup is shown in Fig. 4. A Bruker Avance spectrometer and Bruker imaging probe (Micro2.5 probehead and gradient system with bird-cage RF coil) are used at 9.4 T (400 MHz, ^{1}H). The sample was tap-water in a cylindrical glass tube. Various dimensions of water samples used in this work are listed in Table 1.

The MMME4 sequence in Fig. 1 is used for 1-D imaging. Both MMME4 and MMME5 in Fig. 2 are used for 2-D imaging. Other experimental parameters used in the experiments are also summarized in Table 1.

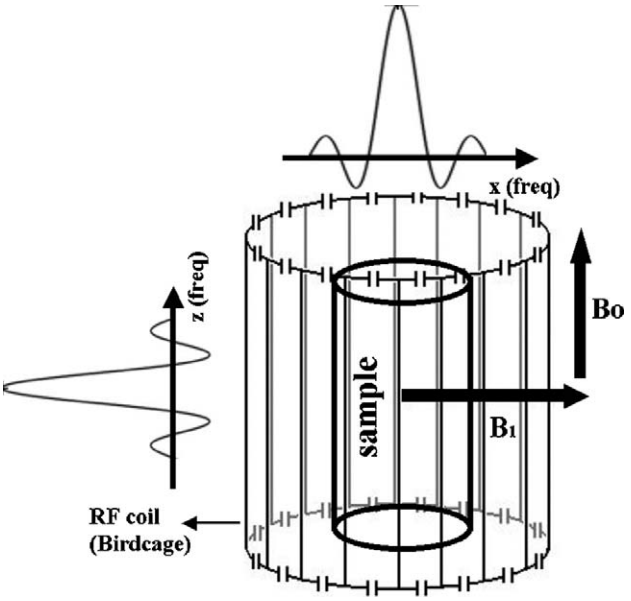

Fig. 4. A schematic diagram of the experimental setup. Two sinc functions along the x and z direction illustrate the frequency selectivity of a square RF pulse on the sample when a constant gradient field is applied along the each direction. A cylindrical water sample appears as an infinitely long sample along the z direction and circular along the x direction.

3.2. 1-D imaging

To verify the essential feature of our proposed method for 1-D image reconstruction from different echoes of the MMME sequence, we performed the MMME4 (4 RF pulses) sequence: [α_1–τ_1–α_2–τ_2–α_3–τ_3–α_4–acquisition] in the presence of a constant field gradient at 9.4 T (400 MHz, ^{1}H), where α_n's and τ_n's are RF flip angles and the delays ($\tau_2 = 3\tau_1$, $\tau_3 = 9\tau_1$) between the pulses, respectively. The phase of all RF pulses was set to zero.

First, a reference scan to obtain information of the off-resonance contribution (f^{echo}) was performed using sample A. A constant magnetic field gradient of 10 G/cm along the z direction is applied during the pulse and the acquisition period. Along the z direction, a sample appears as an infinitely long sample (i.e., homogeneous) and only f^{echo} contributes to the echo shape as shown in Eq. (7). Solid lines in Fig. 5 show echo shape variations for the MMME4 sequence with flip angle combination of [90° −90° −90° −180°] with $\tau_1 = 1$ ms and the z gradient for sample A.

To test the applicability of Eq. (5) and to check the quality of the reconstructed 1-D image profile along the x direction from Eq. (8), the MMME4 sequence with same flip angles and delay (τ_1) was performed with sample B. A constant gradient of 10 G/cm was applied along the x direction. The reason for using samples of different length along the z direction is to minimize RF inhomogeneity issues with the x gradient experiment because the signal from the inhomogeneous region of the RF coil is excited in the x gradient experiment. (In theory, we can compensate for this effect with an accurate knowledge of the RF inhomogeneity profile.) Dashed lines in Fig. 5 show echo shape variations with the x gradient. It is shown that a significant difference between echo shapes exists between the z (flat 1-D profile) and x (circular 1-D profile) gradient experiments.

Fig. 6 compares the shape of each echo between the x gradient experiment and theory. The theoretical shape of each echo is calculated from Eq. (5), which is obtained by convolving each echo in the z gradient experiment (reference scan) with the time domain echo signal from a conventional spin echo 1-D imaging sequence. ([$\pi/2 - \pi$], with the x gradient.) An excellent agreement of echo shape between both cases in Fig. 6 confirms the validity of Eq. (5) in our proposed scheme.

Since our method Eq. (8) involves the division by the spectrum of each echo from a reference scan, we optimized the combination of the RF flip angle to reduce the zero crossings (oscillations) in each echo spectrum, which lead to sharp peaks after the division in the sample profile region. It is found that a combination of [54° −71° −71° −110°] flip angles not only gives less echo amplitude variation but also fewer zero crossings (oscillations) in the spectrum of each echo [13]. (We note that the optimal flip angle for the MMME sequence differs from that of QUEST type sequences because the last pulse was not a π pulse.) Echo shape variations for [54° −71° −71° −110°] flip angles are shown in Fig. 7 in comparison with theoretically calculated echo shape variations for given flip angles.

To reconstruct the 1-D image, each echo from the MMME4 sequence with a constant x gradient is cropped with 100 data points in the time domain (13 sets), centered at $n\tau_1$ time points from the beginning of the acquisition. Each echo is then Fourier transformed and the spectrum of each echo is divided by the spectrum of the corresponding

Table 1
Experimental parameters and samples used in this paper

Pulse sequences (results)	τ_0	τ_1	G_x	ΔG_y, t_{ph}	RF ($\pi/2$) [μs]	ϕ	Sample	Δt (μs)
MMME4 (Fig. 8)		1 ms	10 G/cm		34.5	0	A,B	5
MMME5 (Fig. 10)	1 ms	800 μs	10 G/cm	0.7 G/cm, 150 μs	34.5	0	C,D	10
MMME5 (Fig. 11-B)	1 ms	200 μs	20 G/cm	0.5 G/cm, 100 μs	19.5	0	A	2.5
MMME4 (Fig. 11-A)	1 ms	200 μs	20 G/cm	0.5 G/cm, 100 μs	19.5	0	A	2.5
Sample	A	B	C	D (4 tubes)				
Dia. × length (z), cm	0.75 × 6	0.75 × 1	1 × 5	0.4 × 4, 0.2 × 4				

Δt represents digitization dwell time and ϕ is the phase of RF pulse. t_{ph} refers to the duration of a single phase-gradient lobe.

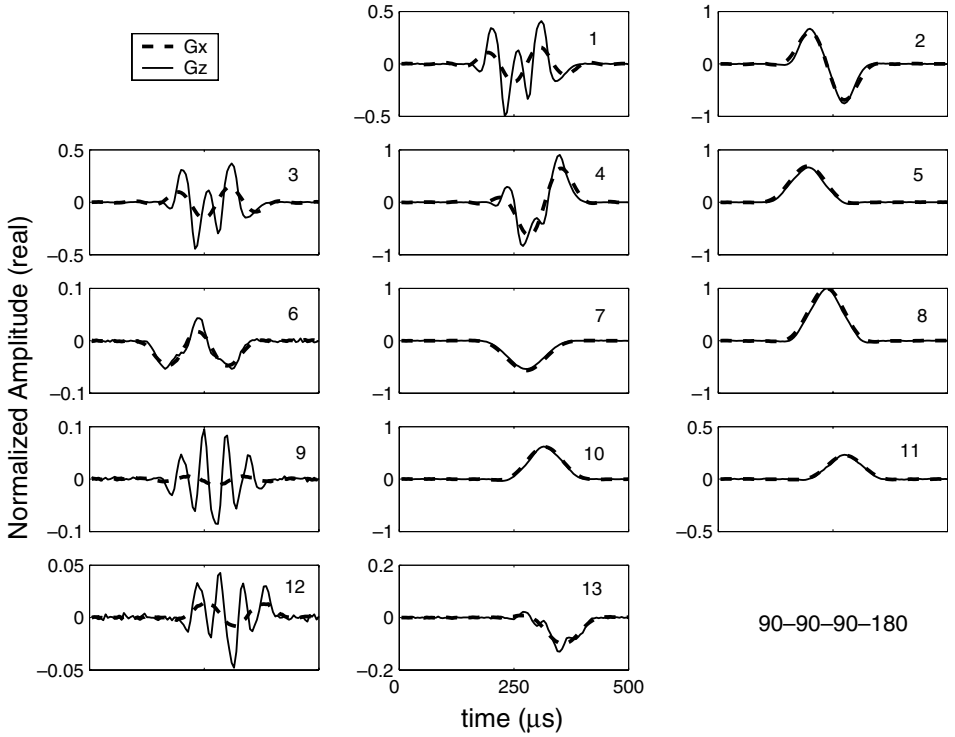

Fig. 5. Echo shape variations for samples with different 1-D profiles. Solid lines represent 13 different echo shapes from the MMME4 [(90° −90° −90° −180°) flip angles] sequence with a constant gradient along the z direction. Dashed lines are along the x direction. Echoes are arranged such that the number in each figure represents the echo number in sequential order during the acquisition. Digitization rate was set to 5 μs and 100 data points were cropped in the time domain for each echo, centered at $n\tau_1 (n = 1–13)$ time points from the beginning of the acquisition after the last pulse.

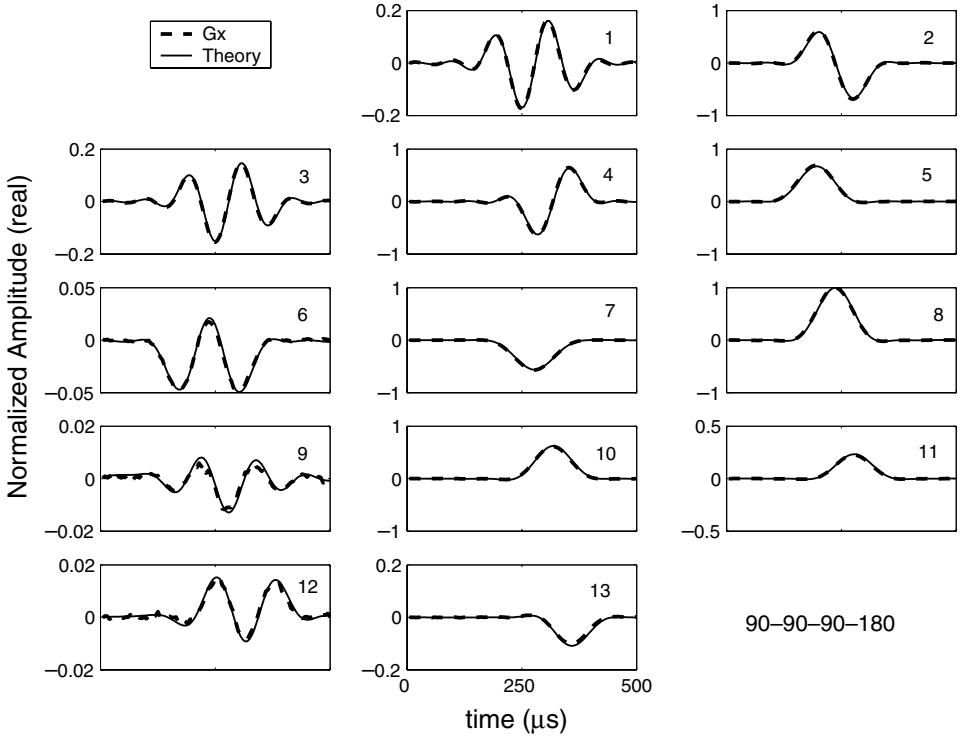

Fig. 6. Dashed lines represent 13 different echo shapes from the MMME4 sequence [(90° −90° −90° −180°) flip angles] with a constant gradient along the x direction for sample A. Solid line is calculated from the convolution of the reference scan (solid lines in the Fig. 5) with the signal from a conventional spin echo 1-D imaging sequence.

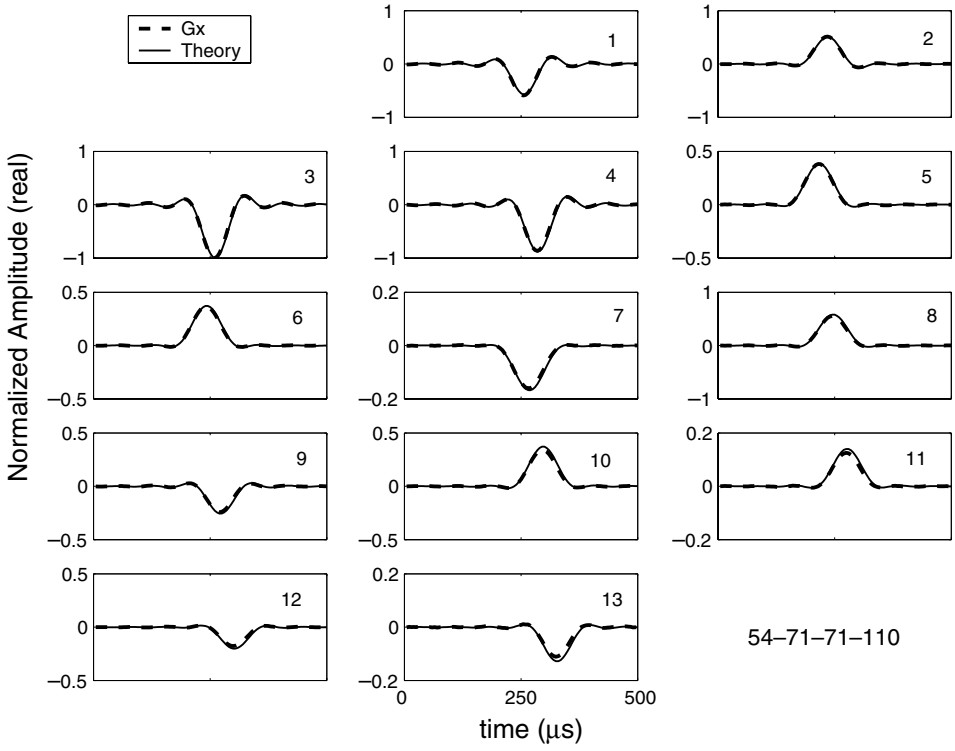

Fig. 7. Plot similar to Fig. 6 with [54° −71° −71° −110°] flip angles.

echo from the reference scan (MMME4 sequence with z gradient) according to Eq. (8) (i.e., $\rho(x) = \mathscr{F}^{-1}(S^{x}_{\text{echo}})/\mathscr{F}^{-1}(S^{z}_{\text{echo}})$). The results of the reconstructed 1-D image profile (solid line) of a water sample inside the cylindrical glass tube are shown in Fig. 8. Spikes from the division by zero values outside the sample regions are removed by applying a top-hat filter. Inset figure (A) shows the expected 1-D profile of the sample obtained from a spin echo sequence with the x gradient, and (B) is the 1-D profile of the 6th echo before applying a top-hat filter. (Spikes outside ~32 kHz bandwidth were filtered out, considering that $\gamma G_x L \sim 31$ kHZ in this experiment. L denotes the dimension of the sample.)

It is important to note that the reference scan experiment along the z gradient with an infinitely long sample can be replaced by theoretically calculated echo shapes for the 1-D image reconstruction [13]. Dashed lines in Fig. 8 show 1-D image profile obtained using theoretical echo shapes, which removes the necessity of an additional experiment for a reference scan.

3.3. 2-D imaging with slice selection

The pulse sequence of 2-D imaging with slice selection is given in Fig. 2. For the MMME5 sequence, five hard pulses are applied with [54° −71° −71° −71° −110°] flip angle combinations [13] and the phase of all pulses was set to zero. τ_1 was varied from 200 to 800 μs with $\tau_2 = 3\tau_1$, $\tau_3 = 9\tau_1$, $\tau_4 = 17\tau_1$. A total of 47 echoes are created and 39 echoes are sampled for image reconstruction. Low amplitude echoes (echo 2, 11, 42–47) are left out for better image reconstruction. Other relevant experimental parameters are summarized in Table 1.

A train of small blipped gradients are switched between successive echoes to phase encode each echo separately. The ordering of encoding k-space used in the experiments (MMME4 and MMME5) follows the encoding scheme described in Fig. 3. Also, 15 high amplitude echoes are sampled during the delays τ_3 and τ_4, and a refocusing gradient lobe is applied at the end of both periods to remove any phase accumulation before the next RF pulse.

For slice selection, Fig. 9 shows magnetization profiles after each pulse with sample C. (Magnetization profiles are obtained by application of each soft pulse for 1 ms followed by spin echo detection with a z gradient.) We observe similar slice selectivity for both soft pulses. A gradient [c] (20 G/cm) in G_y direction is applied to crush the transverse magnetization excited by soft pulses.

For image reconstruction, each echo is cropped with 64 or 96 data points, centered at $n\tau_1$ time points from the beginning of the acquisition and Fourier transformation in the frequency encoding direction is performed. The spectrum of each echo is divided by the spectrum of the corresponding echo from the reference scan (MMME sequence with z gradient only) according to Eq. (8). Second, Fourier transformation is performed in the phase encoding direction. Finally, a top-hat filter is applied to remove spikes outside the image profile region along the frequency encoding direction. A 2-D profile of 1 cm diameter water sample in a cylindrical glass tube and that of 4 tubes (two 4 mm

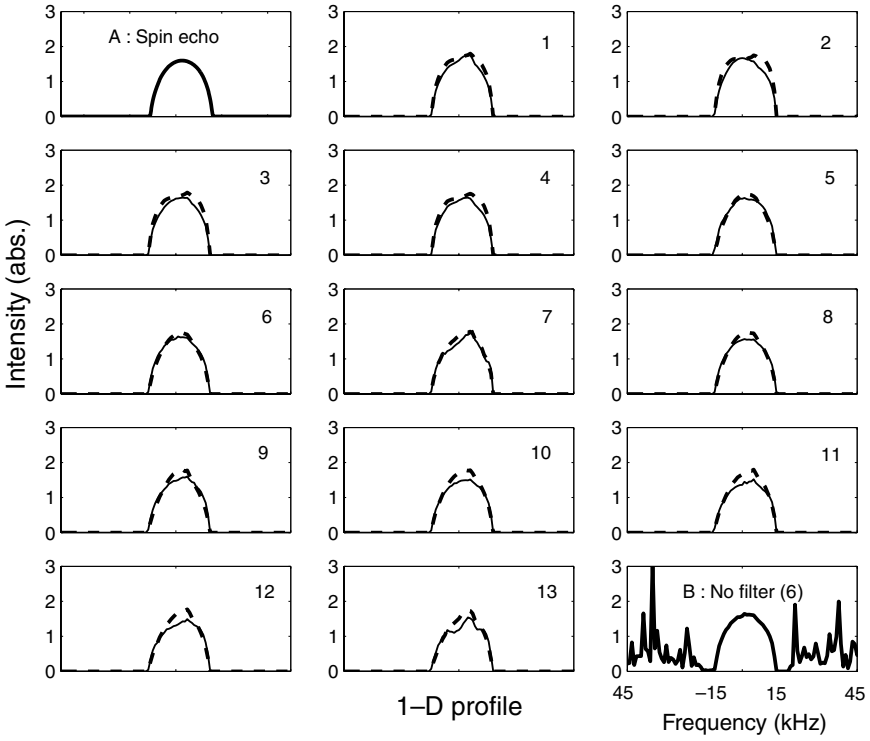

Fig. 8. Reconstructed 1-D image profiles of cylindrical water sample. A combination of $[54°-71°-71°-110°]$ RF flip angles was used with $\tau_1 = 1$ ms. Other relevant experimental parameters are summarized in Table 1. (A) Shows the expected 1-D profile of sample obtained from a spin echo sequence with the x gradient, and (B) is the 1-D profile before applying a top-hat filter. Dashed lines show reconstructed 1-D image profiles using theoretically calculated echo shapes instead of a reference scan.

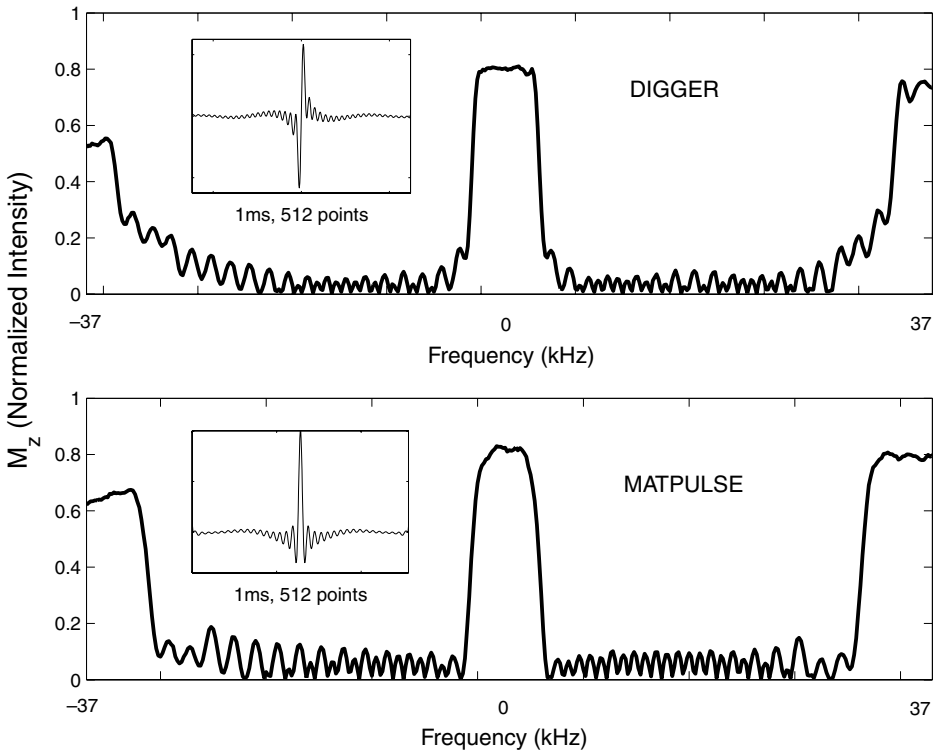

Fig. 9. Experimentally determined z magnetization profile following 1 ms DIGGER pulse and MATPULSE. The signals of M_z for both techniques are normalized with respect to the signal of spin echo sequence (without slice selection) with the same z gradient. Each inset figure shows a soft pulse used for each method. The values of α, β [20] were 3.5 and 3, respectively, and two cycles (-2π to 2π) were used for DIGGER pulse. Slice gradient strength was 10 G/cm to obtain a 1.25 mm slice.

and two 2 mm water tubes) with 5 mm slice selection by DIGGER pulse were obtained.

Fig. 10 shows images reconstructed following this method with experimental parameters listed in Table 1. (A) and (C) are images without echo variation compensation. (B) and (D) show corresponding corrected images with our compensation scheme. Ghosting artifacts along the phase encoding direction (y) in the uncorrected images (A) and (C) are likely due to the amplitude, phase, and shape variations for different echoes. Inhomogeneous image profiles such as bright spots in (A) and (C) seem to originate from a distribution of flip angle across the sample along the frequency encoding direction (x). All images are 96×39 matrix. Their resolutions are 0.3 mm (x, frequency) $\times$ 0.6 mm (y, phase) for (A), (B) and 0.3 mm (x) $\times$ 0.4 mm (y) for (C), (D). The SNR (mean signal intensity in the object divided by the standard deviation of background intensity) was measured to be $\sim$19 and non-uniformity of object intensity (standard deviation of signal intensity divided by the mean signal intensity in the object) was $\sim$6% for the corrected images. Scan time was 45 ms for both cases with $\tau_1 = 800$ μs.

Fig. 11 shows a similar image with $\tau_1 = 200$ μs. To prevent echo overlap, frequency encoding gradient strength was increased to 20 G/cm, and it provided enough echo separation for image processing. However, the shorter period between echoes precluded the previously applied phase encoding gradient due to the switching times. We

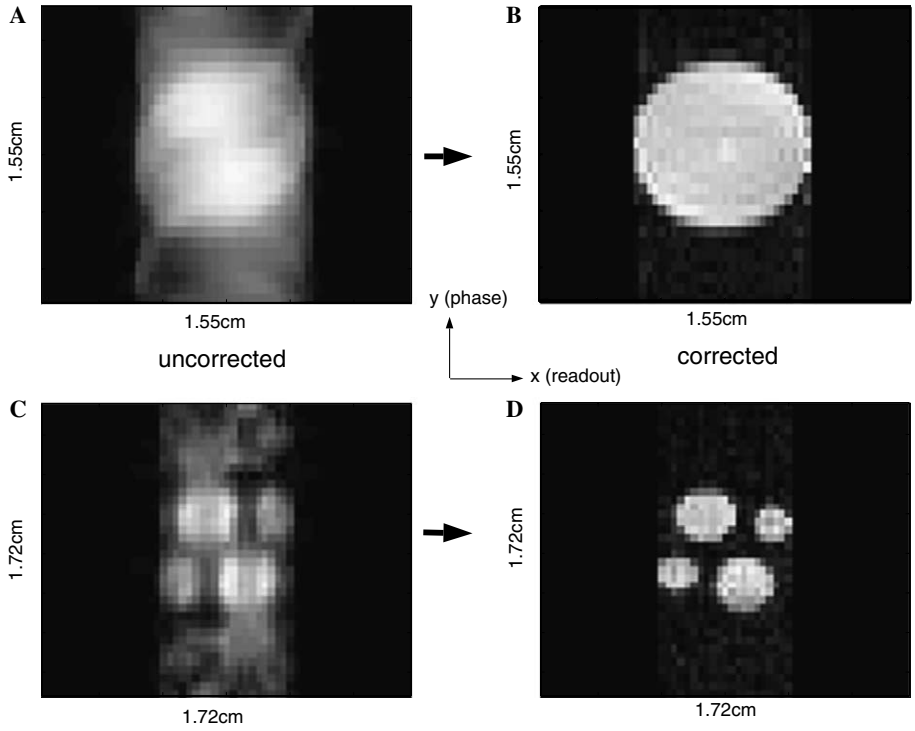

Fig. 10. 2-D imaging with slice selection for $\tau_1 = 800$ μs. All images have a matrix size of 96×39, and resolution of 0.3 mm (x, frequency) $\times$ 0.6 mm (y, phase) and 0.3 mm (x) $\times$ 0.4 mm (y), respectively. (A) and (C) are images without echo variation compensation. (B) and (D) show corresponding corrected images with our technique. Scan time is $54\tau_1 + 2$ ms (DIGGER) = 45 ms for both experiments.

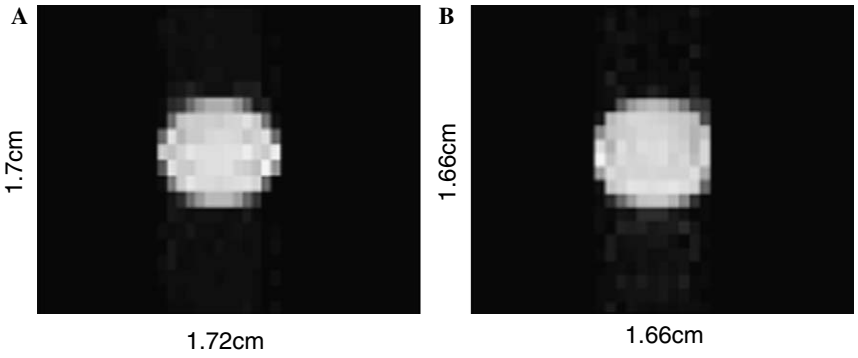

Fig. 11. 2-D half Fourier imaging with slice selection for $\tau_1 = 200$ μs. (A) and (B) have a matrix size of 96×25 and 96×64, respectively, and resolution of 0.5 mm (x) $\times$ 0.9 mm (y), 0.45 mm (x) $\times$ 0.75 mm (y), respectively.

performed half Fourier imaging [25,26] to overcome this difficulty because it removes the need for a high strength phase encoding gradient in the middle of the sequence. For image (A), a 96×13 matrix was obtained in 5 ms for the positive k_y component only with the MMME4 sequence. The negative components were filled using $s(-k) = s^*(k)$ relationship to obtain a 96×25 matrix. The resolution of the image was 0.5 mm (x) × 0.9 mm (y). Image (B), a 96×64 matrix, was obtained in 14 ms with the resolution of 0.45 mm (x) × 0.75 mm (y) with a similar half Fourier method after acquiring a 96×32 matrix with the MMME5 sequence. The SNR of the image was measured to be ~36 for image (A) (MMME4) and ~23 for image (B) (MMME5). Non-uniformity of object intensity was ~3% for the MMME4 and ~7% for the MMME5.

3.4. Discussion

The benefit of our correction technique is clearly demonstrated in Fig. 10. However, it should be noted that the effective field of view in the corrected image is smaller than the field of view set by the digitization time and gradient strength along the readout direction due to the application of a top-hat filter. Other advanced deconvolving algorithms might remove the need for division by zero values in the signal-free region of echo spectrum, thus enabling the use of the full field of view.

Even though a combination of [54° −71° −71° −110°] flip angles is found to provide less variation in echo amplitude and shape, both in experiment and simulation, than [90° −90° − 90° −180°] pulses, it is not clear if there exists a better combination of pulses for general applications of the MMME sequence. While it is known that it is impossible to find a set of flip angles to equalize the amplitude of all echoes even at on-resonance condition, the set of [54° −71° −71° −110°] flip angles is shown to provide the minimum spread of echo amplitudes at on-resonance condition [13], but not necessarily the minimum for echo shape variations. The quality of the MMME sequence will improve with a set of flip angles with the least echo variations.

The limitation in the achievable speed with the MMME imaging sequence mainly lies in two factors. The overlap of adjacent echoes as a result of reduction in the delay between the pulses (τ_1) can deteriorate the quality of reconstructed image profile. Experimentally, we observe an echo width of ~200 μs for a 10 G/cm read out gradient strength. In principle, it is possible to prevent echo overlap from very short delay as echo width is inversely proportional to the applied gradient strength. However, RF power needs to be increased to cover the entire sample range as gradient strength gets larger. For a sufficient excitation of the entire sample with a hard rectangular pulse, it will be desirable to have

$$L \leqslant \frac{2}{\gamma G t_p}, \tag{9}$$

where L is the dimension of the sample, γ is the gyromagnetic ratio, G is the gradient strength and t_p is the RF pulse width. Since the field of view along the readout direction ($\mathrm{FOV_{ro}}$) should be comparable to the sample size of interest,

$$\mathrm{FOV_{ro}} = \frac{1}{\gamma G \Delta t} \geqslant L(\sim \frac{2}{\gamma G t_p}), \tag{10}$$

where Δt is the digitization rate along the frequency direction. Combining Eq. (9 and 10), we can obtain the relevant range of applicable RF pulse widths for MMME imaging, which is

$$2\Delta t \leqslant t_p \sim \frac{2}{\gamma G L}. \tag{11}$$

For instance, ~20 G/cm gradient strength is needed for enough echo separation (echo width of 100 μs) for 200 μs (τ_1) delay (the shortest echo spacing we achieved in our system). Subsequently from Eq. (11), the requirement for RF pulse width follows as 3.2 μs $\leqslant t_p \leqslant$ 24 μs for a 1 cm sample. There exists a trade-off between RF power and the possible maximum speed of the MMME imaging sequence with a given sample size. On the other hand, it is possible to reduce the echo overlap by alternating the phase of RF pulses. It is found that a simple phase alternation of RF pulses ($[0,0,0,0,0] \rightarrow [0,\pi/2,0,\pi/2,0]$) produces $\pi/2$ phase shifts between successive echo signals, which improves the separation of each echo by a factor of two.

Another factor to consider is the switching time of the phase encoding gradient. The phase encoding gradient is smaller than the frequency encoding gradient, and requires less gradient slew rate. Still, it poses a limitation for extremely short sequences. Half fourier imaging (when the image is real) [25] seems to be a good solution to remove the high amplitude phase encoding gradient because only small gradient blips are used to encode half of the k_y space. We did not observe any obvious artifacts in Fig. 11 using half fourier technique with the MMME imaging sequence for a static sample, which indicates that there are no detrimental local phase errors from the MMME imaging sequence itself. However, it might be worthwhile to apply advanced local phase recovery algorithms, such as POCS along with the half fourier MMME imaging sequence in the presence of fast flow [26].

In short, faster and higher signal-to-noise ratio one-shot imaging can be performed at the cost of high power RF pulses with the MMME imaging sequence proposed in this paper.

4. Conclusion

In conclusion, we have presented a fast imaging method based on the MMME sequence. Echo shape variations from a constant frequency encoding gradient during the RF pulses is successfully deconvolved from the true 1-D image profile, and this method is extended to 2-D imaging with phase encoding and slice selection. Fast imaging

($\leqslant$10 ms) is achieved at sub-millimeter resolution. This method could be useful in capturing real-time events such as the beating of a heart or muscle flexings, etc., though motion dependent signal dephasing during the pulse train may deteriorate image quality for in vivo applications. It may also be used for ex situ NMR imaging applications where a non-switchable gradient field exists such as rapid well-logging.

The authors thank G. Leu for helpful discussions.

References

[1] P. Mansfield, Multi-planar image formation using NMR spin echoes, J. Phys. C 10 (1977) L55.
[2] A. Haase, J. Frahm, D. Matthaei, W. Hanicke, K.-D. Merboldt, FLASH imaging-rapid NMR imaging using low flip-angle pulses, J. Magn. Reson. 67 (1986) 258.
[3] J. Hennig, RARE imaging: a fast imaging method for clinical MR, Magn. Reson. Med. 3 (1986) 823.
[4] C.J.R. Counsell, PREVIEW: a new ultrafast imaging sequence requiring minimal gradient switching, Magn. Reson. Imaging 11 (1993) 603.
[5] O. Heid, M. Deimling, W. Huk, QUEST– a quick echo split NMR imaging technique, Magn. Reson. Med. 29 (1993) 280.
[6] R. Jerecic, M. Bock, L.R. Schad, An amplitude optimized single-shot hybrid QUEST technique, Magn. Reson. Imaging 18 (2000) 23.
[7] I.J. Lowe, R.E. Wysong, DANTE ultrafast imaging sequence (DUFIS), J. Magn. Reson. Series B 101 (1993) 106.
[8] L. Zha, I.J. Lowe, Optimized ultra-fast imaging sequence, Magn. Reson. Med. 33 (1995) 377.
[9] D.P. Madio, I.J. Lowe, Ultra-fast imaging using low flip angles and FIDS, Magn. Reson. Med. 34 (1995) 525.
[10] J. Hennig, M. Hodapp, Fast imaging using burst excitation pulses, in: Proceedings of 7th Meeting SMRM, San Francisco, 1988, p. 238.
[11] J. Hennig, M. Mueri, Burst imaging, MAGMA 1 (1993) 39.
[12] J. Hennig, Echoes—how to generate, recognize, use or avoid them in MR-imaging sequences, Concepts Magn. Reson. 3 (1991) 179.
[13] Y.-Q. Song, X.-P. Tang, A one-shot method for measurement of diffusion, J. Magn. Reson. 170 (2004) 136.
[14] A. Sodickson, D.G. Cory, A generalized *k*-space formalism for treating the spatial aspects of a variety of NMR experiments, Prog. NMR Spectrosc. 33 (1998) 77.
[15] R.J. Nelson, Y. Maguire, D.F. Caputo, G. Leu, Y. Kang, M. Pravia, D. Tuch, Y.S. Weinstein, D.G. Cory, Counting echoes: application of a complete reciprocal-space description of NMR spin dynamics, Concepts Magn. Reson. 10 (1998) 331.
[16] X.-P. Tang, E.E. Sigmund, Y.-Q. Song, Simultaneous measurement of diffusion along multiple directions, J. Am. Chem. Soc. 126 (2004) 16336.
[17] E.E. Sigmund, Y.-Q. Song, Multiple echo diffusion tensor acquisition technique, Magn. Reson. Imag, 24 (1) (2006) 7.
[18] Y.-Q. Song, Categories of coherence pathways in the CPMG sequence, J. Magn. Reson. 157 (2002) 82.
[19] M.D. Hurlimann, Diffusion and relaxation effects in general stray field NMR experiments, J. Magn. Reson. 148 (2001) 367.
[20] D.M. Doddrell, J.M. Bulsing, G.J. Galloway, W.M. Brooks, J. Field, M. Irving, H. Baddeley, Discrete isolation from gradient-governed elimination of resonances. DIGGER, a new technique for in vivo volume-selected NMR spectroscopy, J. Magn. Reson. 70 (1986) 319.
[21] G.J. Galloway, W.M. Brooks, J.M. Bulsing, I.M. Brereton, J. Field, M. Irving, H. Baddeley, D.M. Doddrell, Improvements and extensions to the DIGGER technique for performing spatial selective excitation, J. Magn. Reson. 73 (1987) 360.
[22] A. Roch, H.H. Raeymaekers, L. Lamalle, Y.V. Haverbeke, R.N. Muller, Optimization schemes for selective excitations: application to the DIGGER pulses, Magn. Reson. Imaging 10 (1992) 465.
[23] G.B. Matson, An integrated program for amplitude-modulated RF pulse generation and re-mapping with shaped gradients, Magn. Reson. Imaging 12 (1994) 1205.
[24] J. Pauli, P.L. Roux, D. Nishimura, A. Macovski, Parameter relations for the Shinnar-Le Roux selective excitation pulse design algorithm, IEEE Trans. Med. Imaging 10 (1991) 53.
[25] P. Margosian, F. Schmidtt, D.E. Purdy, Faster MR imaging: imaging with half the data, Health Care Instr. 1 (1986) 195.
[26] E.M. Haacke, E.D. Lindskog, W. Lin, A fast, iterative partial Fourier technique capable of local phase recovery, J. Magn. Reson. 92 (1991) 126.